Microchimica Acta (2019) 186:789
https://doi.org/10.1007/s00604-019-3839-1

ORIGINAL PAPER

# A coaxial nanocable textured by a cerium oxide shell and carbon core for sensing nitric oxide

Guorong Hou[1] · Yanjing Yun[1] · Minqiang Wang[1] · Ying Wang[1] · Hao Chen[1] · Longcheng Zhang[1] · Feng Wang[2,3] · Qingyou Xia[2,3] · Yang Liu[4] · Zhisong Lu[1] · Shu-Juan Bao[1]

Received: 23 May 2019 / Accepted: 16 September 2019


## Abstract

A corn-like $CeO_2$/C coaxial cable textured by a cerium oxide shell and a carbon core was designed to sense NO. The carbon core possesses high electrical conductivity, and the $CeO_2$ surface delivers excellent electrocatalytic activity. The sensor, typically operated at 0.8 V (vs. Ag/AgCl), exhibits a detection limit of 1.7 nM, which is 4-times lower than that of $CeO_2$ nanotubes based one (at $S/N = 3$). It also displays wide linear response (up to 83 μM), a sensitivity of 0.81 μA $\mu M^{-1}$ $cm^{-2}$, and fast response (2 s). These values are highly competitive to that of a $CeO_2$ tube (0.92 μA $\mu M^{-1}$ $cm^{-2}$ and 2 s). The sensor was used to quantify NO that is released by Aspergillus flavus.

**Keywords** Electrospinning · Voltammetric determination · Biosensor · Aspergillus flavus

## Introduction

Food spoilage can result in large economic losses and cause various diseases, such as dysentery, hepatitis, cancer, and even death [1, 2, 3, 4, 5]. Therefore, detecting such spoilage early is an ongoing and imperative need to ensure food safety worldwide [6, 7]. When several types of agricultural crops begin to spoil, a large amount of the ubiquitous saprotrophic and pathogenic filamentous fungus Aspergillus flavus (*A. flavus*) is produced [8, 9]. Subsequently, small molecules like reactive oxygen and nitrogen species (RONS) will be produced during metabolism of *A. flavus*. Hence, the status of crop storage can be estimated based on the in situ and real-time detection of nitric oxide (NO) [10, 11]. In addition, NO is a representative type of RONS, which is a diffusible bioactive molecule and plays numerous important signaling roles in biological processes [12]. Nevertheless, NO can be quickly oxidized and has a short biological half-life (6 s), thus low concentrations of NO make the real-time, quantitative detection very difficult [13, 14]. Although electron spin resonance (ESR), fluorometry, spectrophotometry, chemiluminescence, and electrochemistry are available NO sensing detection methods, all exhibit some disadvantages and are not completely reliable [15–19]. For instance, ESR requires expensive equipment and the corresponding trapping agent and can only detect paramagnetic materials. Fluorometry has poor repeatability, while spectrophotometry has poor selectivity and requires fresh $HbO_2$ and hysteresis during detection. Chemiluminescence requires additional reagents and has a poor selectivity. As the most promising technique, the electrochemical method has advantages of low-cost, simplicity, fast analysis, miniaturization, and high sensitivity. It provides a

**Electronic supplementary material** The online version of this article (https://doi.org/10.1007/s00604-019-3839-1) contains supplementary material, which is available to authorized users.

✉ Zhisong Lu
zslu@swu.edu.cn

✉ Shu-Juan Bao
baoshj@swu.edu.cn

[1] Institute for Clean Energy and Advanced Materials, School of Materials and Energy, Southwest University, Chongqing 400715, People's Republic of China

[2] State Key Laboratory of Silkworm Genome Biology, Southwest University, Chongqing 400715, People's Republic of China

[3] Chongqing Engineering and Technology Research Center for Novel Silk Materials, Southwest University, Chongqing 400715, People's Republic of China

[4] Institute of Food Science and Technology, Chinese Academy of Agricultural Sciences/Key Laboratory of Agro-Products Processing, Ministry of Agriculture, No.1 Nongda South Road, Xibeiwang, Haidian District 100193, People's Republic of China

Published online: 15 November 2019

remarkable opportunity to achieve in situ real-time detection of NO in complex biological systems [20].

Generally, natural enzymes have a surprising high catalytic activity and specificity [21]. Yet, natural enzymes suffer from the strict operating situation, short lifetime, and poor reproducibility, which limit the development of enzyme-based electrochemical sensor [22]. The construction of various nanomaterials with tailored textures has provided tremendous momentum for different analysis platforms and bioelectrical sensors [23]. Unfortunately, small-sized nanomaterials easily penetrate into *A.flavus* by endocytosis and cause toxicological damage by producing and eliminating RONS, affecting the accuracy of identification [24]. While large-sized materials are more bio-safe and cannot enter *A. flavus*, they are unable to detect target molecules effectively due to insufficient activity [25, 26]. Inspired by the unique natural structure of corn, the assembly of tiny nanoparticles on a solid fiber core can maintain their excellent reactivity and can also prevent them from entering *A. flavus* and affecting the accurate measurement of NO. Furthermore, the conductive fiber core has fast response.

Hence, in this work, the $CeO_2$ was selected as the electroactive nanomaterial due to its reversible redox reaction between $Ce^{3+}$ and $Ce^{4+}$, boosted catalytic activity, and excellent adsorption and reactivity toward NO [27]. As the inspiration for engineering the unique fiber structure, we considered electrospinning technique to construct the core-like $CeO_2$/C coaxial cable. By regulating the solution composition, electrospinning parameters, and calcination condition, a unique corn-like coaxial cable textured by cerium oxide shell and carbon core ($CeO_2$/C) was successfully fabricated. As shown in Scheme 1, owing to the high conductivity of the carbon core and excellent activity of $CeO_2$ surface, the $CeO_2$/C based biosensor exhibits a satisfactory detection limit, which is lower than 4 times that of $CeO_2$ nanotubes. It has excellent selectivity, good sensitivity (0.92 μA $\mu M^{-1}$ $cm^{-2}$), fast response time (2 s). An obvious current response was also observed when our designed $CeO_2$/C coaxial cable was used to detect NO released from *A. flavus*, which reveals that the coaxial cable structure can provide an excellent analytical platform for biological detection.

## Experimental section

### Reagents and chemicals

Cerium chloride heptahydrate ($CeCl_3 \cdot 7H_2O$, 99.5%), polyvinyl pyrrolidone (PVP, MW = 1,300,000), citric acid anhydrous ($C_6H_8O_7$, 99.5%), N,N-Dimethylformamide (DMF, 99.5%), absolute ethanol ($C_2H_5OH$, 99.7%), uric acid (UA, 99%), dopamine (DA, 98%), ascorbic acid (AA, 99%), calcium chloride anhydrous ($CaCl_2$, 96%), potassium nitrate ($KNO_3$, 99%), sodium carbonate ($Na_2CO_3$, 99.5%), potassium superoxide ($KO_2$, 96.5%), pendimethalin (PE, 99%), 2,2-bis (p-chlorophenyl)-1,1,-trichloroethan (DDT, 100 μg/mL), hydroquinone (HQ, 99.5%), 3-hydroxy-5-methylisoxazole (HY, 99.8%), catechol (CA, 99%), quercetin (QU, 99.5%), histamine (HI, 96%), mercury chloride (99.5%), cadmium nitrate tetrahydrate (99%), lead chloride, phosphate buffered saline (PBS, 0.01 M, pH = 7.4), polysorbate (Tween-80), cinnamic aldehyde (CIN, $C_9H_8O$, 99.5%) were bought from Aladdin Reagent in China (https://www.aladdin-e.com). Nafion (5 wt%) and hemoglobin (Hb) were bought from Sigma-Aldrich (https://www.sigmaaldrich.com/china-mainland.html). Tween-80 was of cell culture grade. Other chemicals were of analytical grade and used directly without any purification. In all experiments, deionized water (18.2 MΩ·cm) was used.

### Apparatus and characterization

Field emission scanning electron microscopy (FESEM, JSM-7800F) and transmission electron microscopy (TEM, JEOL-2100) were used to observe the morphology of the samples. The crystal structure of all samples obtained in our work was characterized by powder X-ray diffraction (XRD, Shimadzu XRD-7000) with Cu Kα source radiation. Raman spectrum (Renishaw, UK) was recorded using an Invia Refl under ambient conditions. Thermo Gravimetric Analyzer (TGA, Q50, USA) was used to study the thermal properties of the samples. The surface information of samples was obtained from X-ray photoelectron spectroscopy (XPS, Escalab 250xi, USA). The electrospinning apparatus was constructed with a high voltage power supply (DW-P503-1 AC, Dongwen, China), receiving roller (21K6RA-C), and syringe pump (Harvard apparatus U.S.A.). The electrochemical tests were performed on the CHI660 electrochemical workstation from CHI Instruments Inc.

### Preparation of the $CeO_2$/C, $CeO_2$ nanotubes and carbon nanofibers

First, 2 mmol $CeCl_3 \cdot 7H_2O$, 2 mmol $C_6H_8O_7$, and 1.0 g PVP were dissolved in 10 mL DMF to form a homogeneous solution under constant stirring at room temperature for 12 h. Then, the solution was filled into a plastic syringe with 22-gauge needle to provide 25 kV at 0.5 mL $h^{-1}$, and the receiving distance was 16 cm. After drying at 70 °C for 12 h, the precursor was pre-sintered at 200 °C (5 °C $min^{-1}$) for 3 h in air. At last, the sample was annealed in a tube furnace at 800 °C (5 °C $min^{-1}$) for 1 h in $N_2$ atmosphere to obtain the product (noted as $CeO_2$/C). Carbon nanofibers (carbon NFs) were also synthesized using the procedure, except without $CeCl_3 \cdot 7H_2O$ in the precursor solution. In addition, $CeO_2$

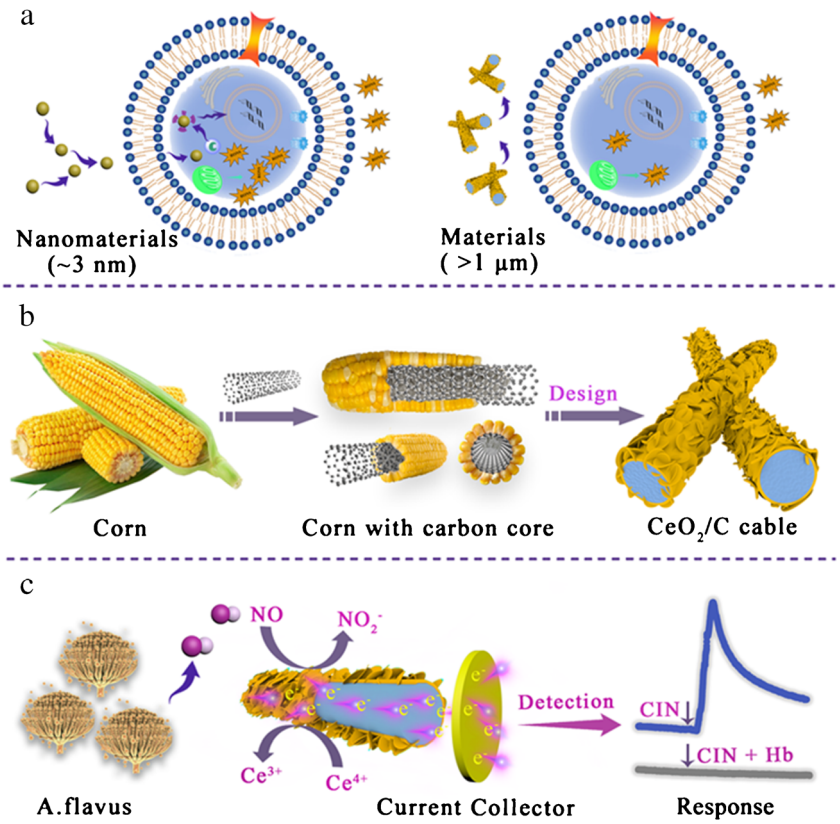


**Scheme 1** (**a**) The effect of materials with different size on the RONS releasing from *A. flavus*; (**b**) Inspiration and design of $CeO_2$/C coaxial cable; (**c**) Oxidation mechanism and detection process of NO released from *A. flavus*

nanotubes were also prepared following the same process but were calcinated in air instead of nitrogen.

### Fabrication of modified electrode

In our work, a working electrode was prepared by the following process. A polishing glassy carbon electrode (GCE, 3 mm in diameter) with 300 and 50 nm alumina slurry to obtain a clean and mirror-like surface, then 5 μL suspension of the sample (2 mg $mL^{-1}$) was dropped onto the GCE. After drying in air at room temperature, 5 μL 0.5% Nafion was used to covered the surface of the modified GCE. A three-electrode system (Ag/AgCl reference, platinum wire counter electrode and working electrode) was used to detect the electrochemical performance of the materials.

### Preparation of nitric oxide

According to previous literature [28], saturated NO in 0.01 M PBS solution was prepared. First, the apparatus was set up and degassed with highly pure nitrogen for 0.5 h. Then, 2 M $H_2SO_4$ was added to saturate the $NaNO_2$ solution for generating NO gas. In order to remove oxygen and nitrogen oxides, NO was successively passed through the saturated KOH solution at 10% (*w*/*v*) and 2.5% (w/v) to obtain approximately 1.8 mM saturated NO at 20 °C.

### Aspergillus flavus culture

Aspergillus flavus GZ-6 was provided by Institute of Agro-Products Processing Science and Technology, Chinese Academy of Agricultural Sciences, P. R. China. As a suitable liquid medium, yeast extract sucrose (YES) broth was prepared by mixing 20 g yeast extract, 150 g sucrose, 3 g potassium nitrate, 0.5 g magnesium sulfate, and 1 L water at 30 °C under constant shaking (200 rpm) and then incubated for Aspergillus flavus (*A. flavus*) growth. The media sample was stored in a refrigerator at 4 °C.

## Results and discussion

### Characterization of materials

The microstructure and morphology of the samples were observed with FESEM and TEM. The images reveal that all precursors of carbon NFs (Fig. S1a), $CeO_2$ and $CeO_2$/C (Fig. S1b) display similar uniform long fibers. Without cerium chloride addition and calcination in nitrogen, uniform carbon NFs is obtained with an average diameter of 110 nm. The results are displayed in Fig. S3. After calcining in air, no products were obtained for the carbon NFs precursor, while uniform nanotubes with an average diameter of 150 nm (Fig. 1a and b) composed of ~20 nm nanoparticles were

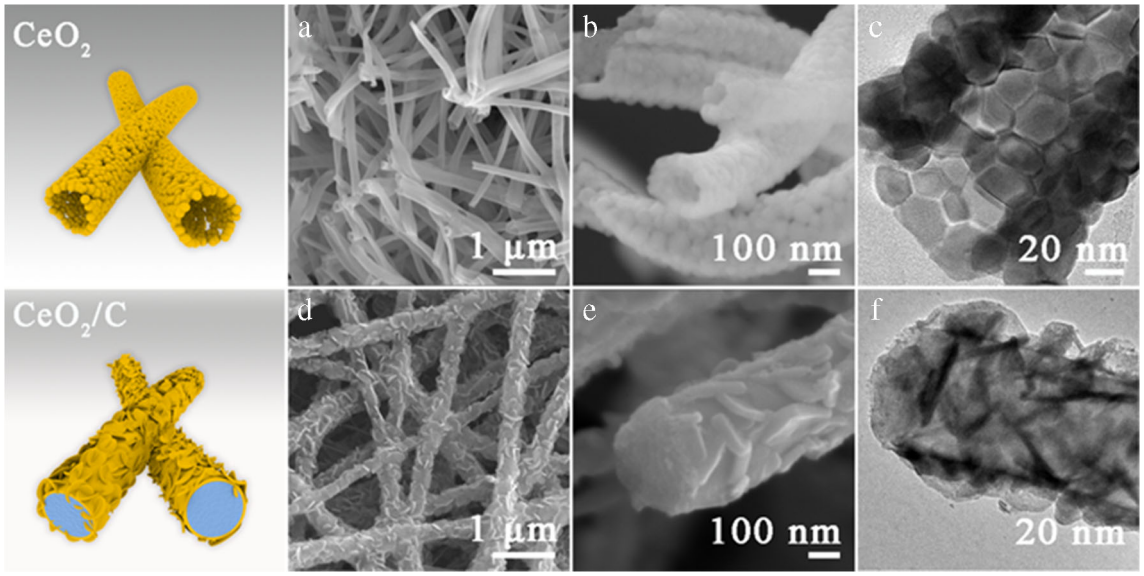


**Fig. 1** (**a**, **b**) FESEM and (**c**) TEM images of $CeO_2$ nanotubes; (**d**, **e**) FESEM and (**f**) TEM images of $CeO_2$/C

formed (Fig. 1c) for the precursor of $CeO_2$. The latter may be due to the movement of metal ions with smaller molecular weight to the surface of fibers and the PVP with high molecular weight molecules occupy the fiber interior during the electrospinning process. After calcination in air, PVP was completely removed, and the metal cations were oxidized into metal oxide. While the sample formed in nitrogen, it still remained solid fibers structure with a diameter of about 250 nm (Fig. 1d), but the surface was very rough. About 90 nm nanosheets consisting of ~4 nm particles were consistently embedded in the surface of the solid core (Fig. 1e and f, Fig. S2). Combined with the sample produced in air, the solid core inside the fiber should be carbon obtained from PVP core.

The crystal structure and phase of $CeO_2$/C and $CeO_2$ were detected by X-ray diffraction (XRD). As displayed in Fig. 2a, the diffraction peaks of both samples well indexed into JCPDS no.43–1002. No diffraction peaks corresponding to other phases or impurities were observed, suggesting that the material is cube phase $CeO_2$ with Fm-3 m space group. Furthermore, the diffraction peaks of $CeO_2$/C are obviously wider and weaker than those of the $CeO_2$ nanotubes, which may due to the smaller nanocrystal size and the absence of carbon [29]. Raman spectroscopy was used to further study the presence of carbon in the materials (Fig. 3b). As reported in literature [30], the Raman peaks of carbon NFs and $CeO_2$/C exhibit two sharp peaks at 1325 and 1580 $cm^{-1}$, which assigned to the D band (amorphous structure) and G band (graphitized structure) of carbon, respectively. The obvious $I_D$ and $I_G$ peaks of $CeO_2$/C further confirmed the coaxial cable structure of $CeO_2$/C, while no D and G peaks were observed in the Raman spectrum of $CeO_2$ nanotubes, indicating that the PVP was decomposed completely. Based on the thermogravimetric analysis (TGA) curves of the samples, the content of carbon in $CeO_2$/C is about 17.55% (Fig. 2c). The Ce 3d XPS spectrum provides surface information about the evolution of $Ce^{3+}$ and $Ce^{4+}$ species in samples under different calcination atmospheres. As shown in Fig. 2d, the peaks centered at 879.6, 884.4 and 902.5 eV for $CeO_2$/C and $CeO_2$ nanotubes are attributed to $Ce^{3+}$, and the peaks around 881.5, 888.0, 897.5, 900.0, 906.5, and 915.9 eV result from $Ce^{4+}$ in both samples. The relative amount of $Ce^{3+}$ was estimated by integration of $Ce^{3+}$ characteristic peaks with respect to the total area of the Ce 3d spectrum. The proportion of $Ce^{3+}$ in $CeO_2$/C was 28.66%, which is about 12% higher than $Ce^{3+}$ in $CeO_2$ nanotubes. The high content of $Ce^{3+}$ on the surface of $CeO_2$/C is mainly due to the inert calcination atmosphere and carbon reduction. It provides numerous active sites for detecting NO [31].

## Electrochemical behavior

Cyclic voltammetry (CV) of the different electrodes was first performed in a solution containing 0.2 M $[Fe(CN)_6]^{3-/4-}$ as the redox probe and 0.1 mol KCl as the supporting electrolyte. As shown in Fig. 3a-c, a pair of well-defined redox peaks of $[Fe(CN)_6]^{3-/4-}$ was observed on carbon NFs, $CeO_2$ nanotubes and $CeO_2$/C coaxial cable electrode, but no obvious redox peaks can be observed on the $CeO_2$ nanotubes electrode. Generally, a small ΔEp (the potential separation of anodic peak to cathodic peak) indicates a fast electron-transfer rate occurred on the corresponding electrode. It is obvious from the CV curves that the ΔEp of performed on $CeO_2$/C coaxial cable is far smaller than that of $CeO_2$ nanotubes, and suggests that the carbon core of $CeO_2$/C coaxial cable significantly fast the electron transfer between $Fe(CN)_6^{3-/4-}$. And the $CeO_2$/C coaxial cable is fully qualified to act as a great promoter that

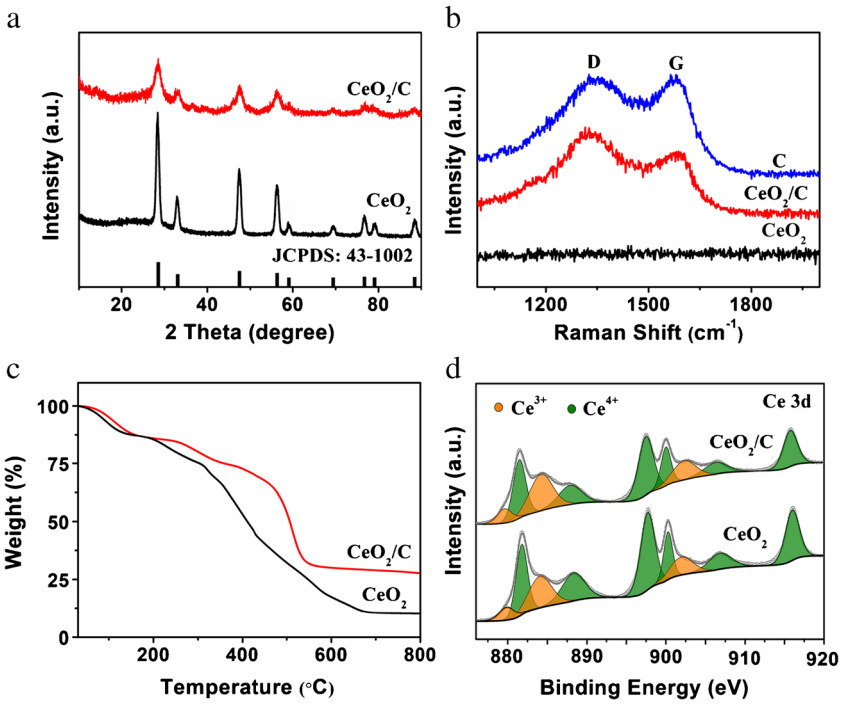


**Fig. 2** (**a**) XRD patterns of $CeO_2$ nanotubes and $CeO_2$/C; (**b**) Raman spectra of carbon NFs, $CeO_2$ nanotubes and $CeO_2$/C; (**c**) TGA curves of $CeO_2$ precursor in air and nitrogen atmosphere; (**d**) XPS high-resolution Ce 3d spectra of $CeO_2$ nanotubes and $CeO_2$/C

can accelerate the electrochemical process successfully. Further, the specific capacitance of the material was calculated using the following formula from the literature [32]:Equation ID=t=t

$$C = \frac{1}{mu(V_c - V_a)} \int_{V_a}^{V_c} IdV$$

Where C (F $g^{-1}$) is the specific capacitance; m (g) is the mass of electroactive materials; υ (mV $s^{-1}$) is the scan rate; $V_c$ and $V_a$ are the high and low potential limits of the CV tests, respectively; and I (A) denotes the instant current on CV curves.

Accordingly, the specific capacitances of carbon NFs, $CeO_2$ nanotubes, and $CeO_2$/C were calculated to be 261.2, 24.4, and 88.6 F $g^{-1}$, respectively. The CV of different

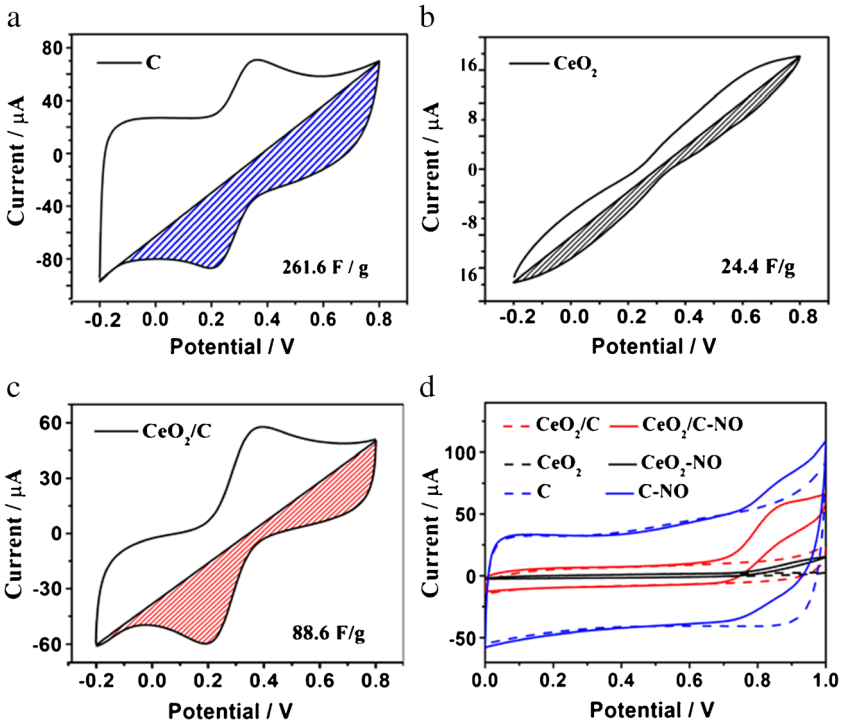


**Fig. 3** (**a** and **b**, **c**) CVs of Carbon NFs, $CeO_2$ nanotubes, and $CeO_2$/C in a 0.2 M $[Fe(CN)_6]^{3-/4-}$ solution containing 0.1 M KCl at 50 $mVs^{-1}$; (**d**) Cyclic voltammetry curves (CVs) of $CeO_2$ nanotubes, $CeO_2$/C and Carbon NFs based electrodes in 0.01 M PBS with and without 3.6 μM NO at 50 $mVs^{-1}$

electrodes in $N_2$-saturated phosphate buffer saline (PBS, 0.01 M, pH = 7.4) at 50 $mVs^{-1}$ are shown in Fig. 3d. Without the addition of NO, all CV curves from different electrodes exhibit a similar rectangular shape within the measured potential range, indicating their ideal capacitive behavior and no any electrochemical reaction. The area of CV curves for $CeO_2$ nanotubes, $CeO_2$/C, and carbon NFs in PBS is consistent with the above calculated results. Obvious current response peaks were observed in three different electrodes with 3.6 μM NO in PBS, which resulted from the oxidation of NO. Although the carbon NFs delivered the largest specific capacitance among the three electrodes, its response current is quite weak due to the insufficient catalytic activity of carbon toward NO. In addition, the large specific surface area of carbon NFs electrode induced a large background current, greatly decreasing its sensitivity. Comparatively, a well-defined NO oxidation peak is observed clearly in the CV curves of $CeO_2$ nanotubes, suggesting the good electrocatalytic activity of $CeO_2$ toward NO. More significantly, a far higher NO oxidation peak was obtained from the $CeO_2$/C electrode, which further demonstrates that the unique coaxial cable structure of corn-like $CeO_2$/C provides a sensitive electrocatalytic surface and improved conductivity. As the scan rate increased in the range of 50~300 $mVs^{-1}$, the current of $CeO_2$/C-based electrode increased linearly (Fig. S4), which implies that the electrochemical reaction on this electrode is a surface-controlled electron transfer process. And the tiny nanoparticles on the surface of $CeO_2$/C coaxial cable offer remarkable activity toward NO.

In order to explore the feasibility of the material-based sensors to detect NO deeply, amperometric i-t measurements were carried out at 0.8 V in 5 mL 0.01 M PBS (pH =7.4). The results are displayed in Fig. 4a and b, a typical stepwise current response with successive increasing NO concentration is observed both of $CeO_2$ nanotubes and $CeO_2$/C, in which 95% of the steady-state current was reached within 2 s. From the corresponding linear calibration plot in Fig. 4c and d, the $CeO_2$ nanotubes-based sensor delivered a high sensitivity (0.92 μA $\mu M^{-1}$ $cm^{-2}$, the linear fitting correction coefficient $R^2 = 0.997$) and low detection limit (7.03 nM, S/$N$ = 3)). It is comparable to those reported biosensors. As expected, a larger linear response range ($5.19 \times 10^{-9}$ to $8.3 \times 10^{-5}$ M), lower detection limit (1.73 nM, S/N = 3), and better sensitivity (0.81 μA $\mu M^{-1}$ $cm^{-2}$, $R^2 = 0.997$) was acquired by the $CeO_2$/C-based electrochemical sensor. More detailed comparisons are summarized in Table S1.

Excellent selectivity and long-term stability are especially important for constructing an effective electrochemical biosensor. UA, AA, DA, $O_2^{\bullet-}$, $Ca^{2+}$, $NO_3^-$, $CO_3^{2-}$, DDT, PE, HY, QU, HQ, CA, AN, $Hg^{2+}$, $Cd^{2+}$, and $Pb^{2+}$ which will influence the accurate detection of our designed sensor were added in the *A. flavus* mycelial suspension and tested in same condition [33]. And they may be oxidized together with NO on the surface of the electrode to cause signal interference. As shown in Fig. 5a, the $CeO_2$/C sensor displayed an obvious amperometric response in the presence of 1 μM NO, while very weak current responses toward 2 μM UA, AA, DA, $O_2^{\bullet-}$, $Ca^{2+}$, $NO_3^-$, $CO_3^{2-}$, DDT, PE, HY, QU, HQ, CA, HI, $Hg^{2+}$, $Cd^{2+}$, and $Pb^{2+}$ can be observed, even can be negligible. It suggested the good selectivity of $CeO_2$/C sensor toward NO. In order to estimate the long-term stability of our designed biosensor, the $CeO_2$/C electrode was placed in air at room temperature for 4 weeks and used to detect NO one times

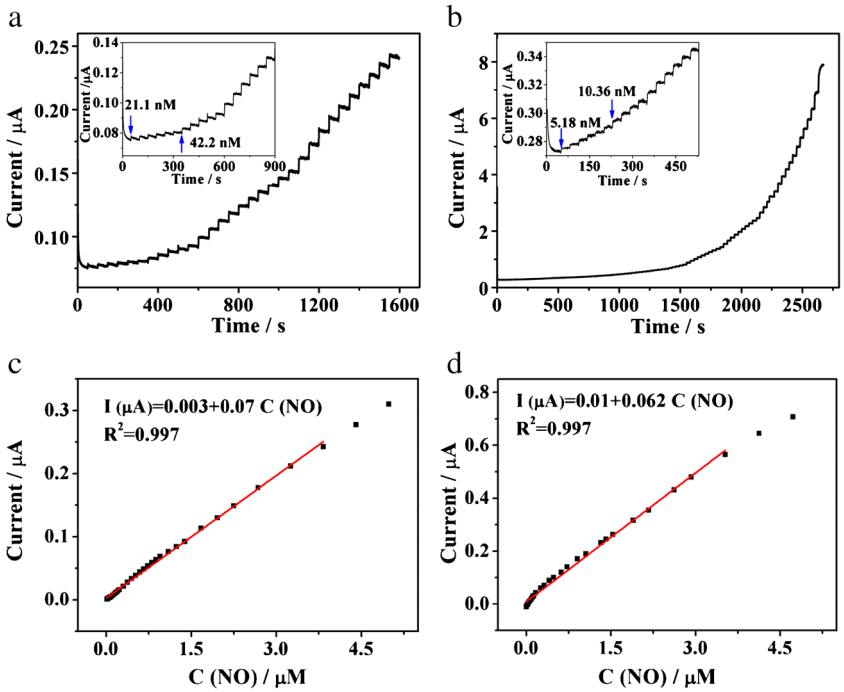


**Fig. 4** (**a**, **b**) Chronoamperometric responses and (**c**, **d**) linear calibration plot of $CeO_2$ nanotubes and $CeO_2$/C based sensors upon continuous injection of NO at an applied potential of 0.8 V in 0.01 M PBS

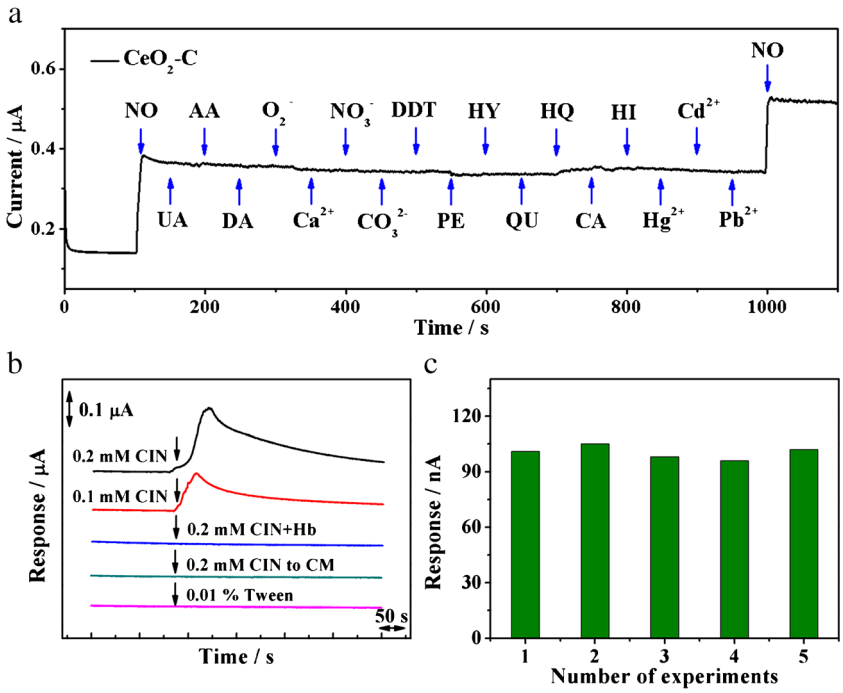


**Fig. 5** (**a**) The amperometric responses of the $CeO_2$/C sensor to the addition of NO, DA, AA, UA, $CaCl_2$, $KNO_3$, $Na_2CO_3$, $O_2^{\bullet-}$, DDT, PE, HY, QU, HQ, CA, HI, $Hg^{2+}$, $Cd^{2+}$ and $Pb^{2+}$ in 0.01 M PBS at 0.8 V, respectively; (**b**) Electrochemical response of $CeO_2$/C sensor for real-time detecting NO released from *A. flavus* under different concentration drug stimulations; (**c**) Repeatability of real-time detection in 0.2 mM CIN solution

per week. And it was found that the catalytic performance of $CeO_2$/C was still maintained 93.46% of the initial detection after 4 weeks, thus confirming its sustained catalytic performance and good stability (Fig. S5).

In our work, *A. flavus* was selected as the model biological sample to estimate the in situ real-time monitor ability of our designed $CeO_2$/C-based sensor for agricultural products storage. Cinnamaldehyde (CIN), an acrolein derivative, was selected as a functional drug to stimulate A.flavus to release NO. Tween-80 is a pharmaceutical solvent of CIN. Based on the results are shown in Fig. 5b, Tween-80 and CIN-Tween-80 did not show any chronoamperometric signal response in 0.01 M PBS. However, when CIN-Tween-80 was added to the detection system containing *A. flavus*, an obvious response current was observed. And the response current stimulated by 0.2 mM CIN was 180 nA, which is about 1.78 times than that using 0.1 mM CIN. In addition, when 0.2 mM CIN-Tween-80 and 1.5 mM Hb mixed solution was added to the detection system containing *A. flavus*, no obvious current response was generated, because NO can react with Hb quickly and mask its reaction with $CeO_2$/C. This result further proves that NO released from *A. flavus* can be effectively detected by our designed $CeO_2$/C cable-based sensor. Moreover, the relative standard deviations (RSD) of current responses of five identical experiments were determined (Fig. 5c) to test the sensor's repeatability. An RSD less than 3.49% reveals that $CeO_2$/C sensor can be applied for the practical determination of NO released from *A. flavus*.

## Conclusions

In this featured work, a unique corn-like $CeO_2$/C coaxial cable textured by a cerium oxide shell and carbon core was designed and engineered using a controllable electrospinning technology and subsequent calcination process. When used to detect NO, $CeO_2$/C performed a low detection limit, wide linear range, fast response time and good reproducibility, which is attributed to excellent activity of the small-sized $CeO_2$ surface and high conductivity of the carbon core. In addition, in situ monitoring NO released from *A.flavus* under drug stimulation was achieved with our designed biosensor, further indicating its great capability for real-time and sensitive detection. This work demonstrates that the construction of nanomaterials with tailored textures is significant to design an excellent sensing platform for food security detection.

**Acknowledgements** This work is financially supported by National Key R&D Program of China (2017YFC1600900), the National Natural Science Foundation of China (21972111, 21773188), Natural Science Foundation of Chongqing (cstc2018jcyjAX0714), Chongqing Engineering Research Center for Micro-Nano Biomedical Materials and Devices, Chongqing Key Laboratory for Advanced Materials and Technologies.

## Compliance with ethical standards

**Conflict of interest** The authors declare that they have no competing interests. This article does not contain any studies with human or animal subjects. Informed consent was obtained from all individual participants include in the study.

## References


1. Xu X-Y, Lian X, Hao J-N, Zhang C, Yan B (2017) A double-stimuli-responsive fluorescent Center for Monitoring of food spoilage based on dye covalently modified EuMOFs: from sensory hydrogels to logic devices. Adv Mater 29(37):1702298
2. Ma X, Mau M, Sharbel TF (2018) Genome editing for global food security. Trends Biotechnol 36(2):123–127
3. Godfray HCJ, Beddington JR, Crute IR, Haddad L, Lawrence D, Muir JF, Pretty J, Robinson S, Thomas SM, Toulmin C (2010) Food security: the challenge of feeding 9 billion people. Science 327(5967):812–818
4. Kumar D, Kalita P (2017) Reducing postharvest losses during storage of grain crops to strengthen food security in developing countries. Foods 6(1):8
5. Alum EA, Urom S, Ben CMA (2016) Microbiological contamination of food: the mechanisms, impacts and prevention. Int J Sci Technol Res 5(3):65–78
6. Rawat S (2015) Food spoilage: microorganisms and their prevention. Asian J Plant Sci Res 5(4):47–56
7. Ma Z, Chen P, Cheng W, Yan K, Pan L, Shi Y, Yu G (2018) Highly sensitive, printable nanostructured conductive polymer wireless sensor for food spoilage detection. Nano Lett 18(7):4570–4575
8. Jaime-Garcia R, Cotty PJ (2018) Crop rotation and soil temperature influence the community structure of Aspergillus flavus in soil. Soil Biol Biochem 42(10):1842–1847
9. Hedayati MT, Pasqualotto AC, Warn PA, Bowyer P, Denning DW (2007) Aspergillus flavus: human pathogen, allergen and mycotoxin producer. Microbiol 153(6):1677–1692
10. Castello PR, Woo DK, Ball KA, Wojcik J, Liu L, Poyton RO (2008) Oxygen-regulated isoforms of cytochrome c oxidase have differential effects on its nitric oxide production and on hypoxic signaling. Proc Natl Acad Sci U S A 105:8203–8208
11. Zhao J, Wang L, Xu D, Lu ZS (2017) Involvement of ROS in nanosilver-caused suppression of aflatoxin production from aspergillus flavus. RSC Adv 7(37):23021–23026
12. Govindhan M, Chen A (2016) Enhanced electrochemical sensing of nitric oxide using a nanocomposite consisting of platinum-tungsten nanoparticles, reduced graphene oxide and an ionic liquid. Microchim Acta 183(11):2879–2887
13. Guo CX, Ng SR, Khoo SY, Zheng X, Chen P, Li CM (2012) RGD-peptide functionalized graphene biomimetic live-cell sensor for real-time detection of nitric oxide molecules. ACS Nano 6(8): 6944–6951
14. Yang T, Zelikin AN, Chandrawati R (2018) Progress and promise of nitric oxide-releasing platforms. Adv Sci 5(6)
15. Davies MJ (2016) Detection and characterisation of radicals using electron paramagnetic resonance (EPR) spin trapping and related methods. Methods 109:21–30
16. Yao HW, Zhu XY, Guo XF, Wang H (2016) An amphiphilic fluorescent probe designed for extracellular visualization of nitric oxide released from living cells. Anal Chem 88(18):9014–9021
17. Murphy ME, Noack E (1994) Nitric oxide assay using hemoglobin method. Academic Press 233:240–250
18. Kim S, Jung H, Lee C, Kim M, Lee Y (2014) Biological application of $RuO_2$ nanorods grown on a single carbon fiber for the real-time direct nitric oxide sensing. Sensors Actuators B Chem 191:298–304
19. Liu H, Weng L, Yang C (2017) A review on nanomaterial-based electrochemical sensors for $H_2O_2$, $H_2S$ and NO inside cells or released by cells. Microchim Acta 184(5):1267–1283
20. Wang M-Q, Ye C, Bao S-J, Xu M-W, Zhang Y, Wang L, Ma X-Q, Guo J, Li C-M (2017) Nanostructured cobalt phosphates as excellent biomimetic enzymes to sensitively detect superoxide anions released from living cells. Biosens Bioelectron 87:998–1004
21. He Y-H, Xiang Y, Yang D-C, Guan Z (2016) Combining enzyme and photoredox catalysis for aminoalkylation of indoles via a relay catalysis strategy in one pot. Green Chem 18(19):5325–5330
22. Wu J, Wang X, Wang Q, Lou Z, Li S, Zhu Y, Li Q, Wei H (2019) Nanomaterials with enzyme-like characteristics (nanozymes): next-generation artificial enzymes (II). Chem Soc Rev 48(4):1004–1076
23. Bao S-J, Li CM, Zang J-F, Cui X-Q, Qiao Y, Guo J (2008) New nanostructured $TiO_2$ for direct electrochemistry and glucose sensor applications. Adv Funct Mater 18(4):591–599
24. Cheng L-C, Jiang X, Wang J, Chen C, Liu R-S (2013) Nano–bio effects: interaction of nanomaterials with cells. Nanoscale 5(9): 3547–3569
25. Wang Y, Wang D, Sun L-H, Xue P, Wang M-Q, Lu Z, Wang F, Xia Q, Xu M-W, Bao S-J (2019) Constructing high effective Nano-$Mn_3(PO_4)_2$-chitosan in situ electrochemical detection Interface for superoxide anions released from living cell. Biosens Bioelectron 133:133–140
26. Nel A, Xia T, Mädler L, Li N (2006) Toxic potential of materials at the nanolevel. Science 311(5761):622–627
27. Matter MT, Furer LA, Starsich FH, Fortunato G, Pratsinis SE, Herrmann IK (2018) Engineering the bioactivity of flame-made ceria and ceria/bioglass hybrid nanoparticles. ACS Appl Mat Interfaces 11(3):2830–2839
28. Li J, Xie J, Gao L, Li CM (2015) Au nanoparticles–3D graphene hydrogel nanocomposite to boost synergistically in situ detection sensitivity toward cell-released nitric oxide. ACS Appl Mat Interfaces 7(4):2726–2734
29. Su Y, Tang Z, Han W, Zhang P, Song Y, Lu G (2014) Influence of the pore structure of $CeO_2$ supports on the surface texture and catalytic activity for CO oxidation. CrystEngComm 16(24):5189–5197
30. Xu Q, Liu H, Du W, Zhan R, Hu L, Bao S, Dai C, Liu F, Xu M (2018) Metal-organic complex derived hierarchical porous carbon as host matrix for rechargeable Na-se batteries. Electrochim Acta 276:21–27
31. Huang Y, Long B, Tang M, Rui Z, Balogun M-S, Tong Y, Ji H (2016) Bifunctional catalytic material: an ultrastable and high-performance surface defect $CeO_2$ nanosheets for formaldehyde thermal oxidation and photocatalytic oxidation. Appl Catal B 181: 779–787
32. Fan Z, Yan J, Zhi L, Zhang Q, Wei T, Feng J, Zhang M, Qian W, Wei F (2010) A three-dimensional carbon nanotube/graphene sandwich and its application as electrode in supercapacitors. Adv Mater 22(33):3723–3728
33. Li J, Li J, Lu Z, Liu Y, Li CM (2015) Transient transmembrane secretion of $H_2O_2$: a mechanism for the citral-caused inhibition of aflatoxin production from Aspergillus flavus. Chem Commun 51(98):17424–17427